A Novel Cooling System for LED Module Using an Ultrasonic Piezoelectric Microjet

Chien-Ping Wang* and Ming-Hung Hsiao

Department of Mechanical Engineering, National Taipei University of Technology, Taipei, Taiwan.

ABSTRACT

A novel active cooling design for power LED modules integrated with an ultrasonic piezoelectric microjet is investigated in this study. The cooling performance of a microjet was analyzed under varying distances, driving voltages, and operating currents to optimize heat dissipation in the LED module. The experimental results show that the optimal cooling performance is obtained at D=50 mm under varying operating currents and driving voltages. The slopes between chip temperature and driving voltage show approximately linear relationship. The temperature non-uniformity on the LED module is found to decrease with driving voltages but increase with operating current. At high heat power of 4.75 W, the microjet significantly reduced chip temperature by 21.5 °C and increased efficiency by 20% compared to a LED module that used a heat sink. The Nusselt number increased from 7.0 to 9.8 as driving voltage was increased from 10 to 20 V. The present experimental results are useful for designing a high efficient active cooling system for power LED modules.

Keywords: Piezoelectric, Microjet, LED, Efficiency

應用微型超音波壓電噴嘴於發光二極體模組之散熱設計

王建評* 蕭銘宏

國立台北科技大學機械工程系

摘 要

本論文應用一微型壓電式噴嘴於高功率 LED 模組之散熱設計,探討在不同距離、噴嘴驅動電壓、及操作電流下之最佳散熱條件。實驗結果發現在距離為 50mm, LED 模組在不同的驅動電壓及電流下得到最佳效能,溫度與驅動電壓間的關係呈現線性關係且斜率與電流及距離有關。溫度不均勻性隨著噴嘴的電壓增加而下降,但隨著電流上升而增加。在最佳散熱條件下,在功率 4.75 W下,使用壓電噴嘴可降低晶粒溫度達 21.5 ℃ 並且提升 20%的效率。當驅動電壓由 10V 增加至 20V 時,Nusselt number 由 7.0 增加至 9.8,本文研究可用於結合微型超音波壓電噴嘴及 LED 模組,設計微型化高效率之散熱模組。

關鍵詞:壓電,微型噴嘴,發光二極體,效率

文稿收件日期 109.4.7;文稿修正後接受日期 109.6.29; *通訊作者

I. INTRODUCTION

Micro-cooling devices such as heat pipe [1microchannel heat sink [4, 5], and piezoelectric jets [6-9] have attracted interest due to the rapid growth of miniature electronics devices. The excessive high heat flux and limited space are the major challenges for heat dissipation design. Light emitting diodes (LEDs) are now the most reliable and high efficient light sources for lighting fixtures and portable electronics. The extremely high heat flux generated by LEDs can substantially degrade product reliability and lifespan [10, 11]. Piezoelectric jet is one of the promising candidate for active cooling devices due to its low power consumption and miniature size [12-14]. To achieve high flow rate, piezoelectric fans have to operate under resonant frequency. The purpose is to maximize the deflection of actuator diaphragm [15, 16]. Several studies have reported flow characteristics, consumption, and cooling performance of piezoelectric fans operated below ultrasonic frequency [17, 18]. However, excessive noise is a serious issue of using a piezoelectric fan for electronic cooling. The development of the ultrasonic piezoelectric micro-actuator was a breakthrough in electronic cooling applications.

Some studies have investigated flow characteristics and performance of the ultrasonic microjet in recent years [19-22]. Literature about utilizing the ultrasonic piezoelectric microjet as an active cooling device for power LED module is still absent. The objective of the present study provided the first investigation of using an active cooling design which integrate an ultrasonic microjet (Murata Manufacturing Co., Ltd.) for power LED module. High efficiency, noise reduction, and compact size are the advantages of using the ultrasonic piezoelectric microjet. Compared with other heat dissipation methods, the microiet can enhance forced convective heat transfer coefficient without complicated manufacture processes. The microjet can be integrated with passive cooling devices, such as heat sink, to enhance forced convective heat transferred coefficient. Distances, voltages, and operating currents are investigated to optimize cooling performance of the ultrasonic microjet.

II. Experiments

Figure 1 shows the schematic of using the ultrasonic piezoelectric microjet as an active cooling device of LED module. Four multi-die LED devices are mounted on a 1.9×1.9 cm² hybrid aluminum nitride (AlN) ceramic substrate with solder bond. The hybrid structure of the substrate consists of finite area of AlN and FR4. Each die consisted of eight LED chips. The LED module is then adhesive on an aluminum heat sink to dissipate heat to the surrounding. The heat sink consists of four channels with length, width, height, and thickness of 20 mm, 20 mm, 10mm, and 1.5 mm for each channel, respectively. The operating current of the LED module is from 0.1 A to 0.6 A with constant interval of 0.1 A using Agilent E3632A power supply. The hybrid AlN substrate has advantages of electrical insulation and high thermal conductivity. Thermal expansion coefficient of AlN is comparable to that of a nitride based LED chip. Additional, the hybrid structure of the substrate has the advantages of low cost and easy assembly. Samples used in the present experiments had an area of 1.1×1.1 cm² with square shape.

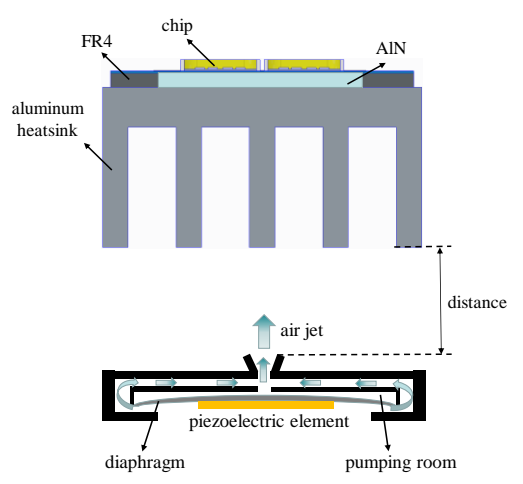


Fig.1. Schematic of using the ultrasonic piezoelectric microjet as an active cooling device

Figure 2 shows the experimental setup to measure chip temperatures on the LED modules. The Instek GPE-1326 power supply is used to provide constant driving voltages to the microjet. Varying distances, driving voltages, and operating currents are compared to

determine the optimal heat dissipation when the microjet is used as an active cooling device of the LED module.

In this experiment, the emissivity of silicone encapsulant is 0.95 [23, 24]. An infrared microscope (CHCT P384-23um) is used to measure the chip temperatures of the LED module. The LED module is placed vertically above the microjet. The distance D represents the gap between the bottom of the heat sink and the jet exit of the microjet. Chip temperatures are analyzed under varying distances, operating currents, and driving voltages. The cooling performance of the microjet of the multi-chip LED module is compared under natural and force convection.

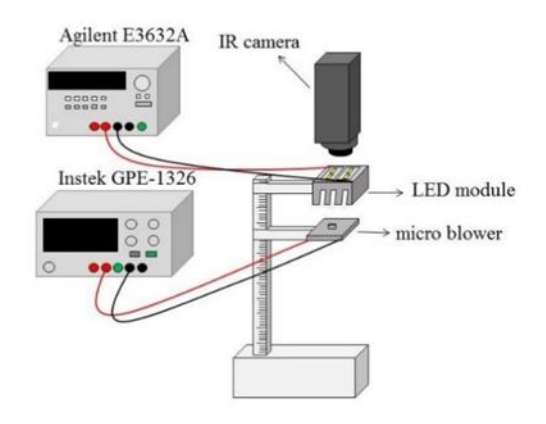


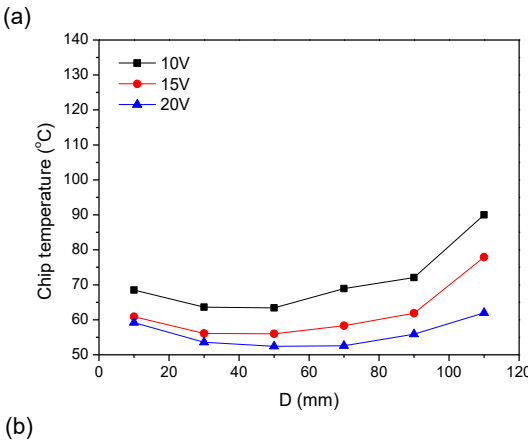
Fig.2. Experimental setup to measure surface temperature of the LED module

III. RESULTS AND DISCUSSION

Figures 3(a) to (c) show the highest chip temperatures on the LED module. Chip temperatures were measured under varying operating currents (0.4 A to 0.6 A) to investigate the cooling performance of the ultrasonic microjet. Fig. 3(a) represented chip temperatures on the LED module at 0.4 A under different driving voltages of 10 V, 15 V, and 20 V of the microjet. The distance is from 10 mm to 110 mm. The experimental results show that chip temperature decreases as D increases from 20 to 50 mm at different driving voltages from 10 V to 20 V. The force convection heat transfer Q can be expressed as follows:

$$Q = hA_a(\Delta T) \tag{1}$$

in which ΔT is the temperature difference between LED module and surrounding, h is the force convective heat transfer coefficient, and A_a is the impinging cooling area on heat sink. A higher jet velocity results in a high convective heat transfer coefficient. The impinging area on the heat sink by jet flow highly depends on distance and jet velocity.



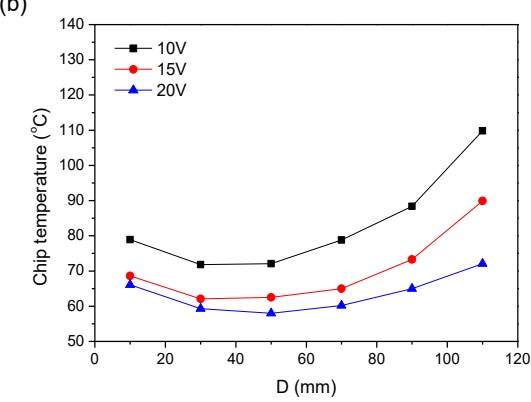


Fig.3. Maximum temperatures of the LED modules under varying distances at operating current (a) 0.4 A (b) 0.5A and (c) 0.6 A

At D=10 mm, impinging area on the heat sink strongly affects force convection heat transfer by jet flow. When the distance is increased from 10 mm to 50 mm, the increment in the impinging cooling area on the heat sink leads to an increment of force convection. Chip temperatures decrease as distance increased from 10 mm to 50 mm under varying driving voltages. When the distance exceeds 50 mm, the decline of jet velocity lead to an increase of chip temperature of the LED module, especially when D≥90 mm. The rate of increase in chip temperature was higher under a low driving voltage than at a high driving voltage due to significant drop in jet velocity. At D=50 mm, the

lowest chip temperatures are obtained at 63.4 °C, 56.0 °C, 52.4 °C under 10 V, 15 V, and 20 V respectively. The maximum temperature difference is about 11 °C as driving voltage increases from 10 V to 20 V. In addition, the highest chip temperatures are obtained at 90.0 °C, 77.9 °C and 62.0 °C under 10 V, 15 V, and 20 V respectively, at D=110 mm. The maximum temperature difference approximated 28 °C. The change in driving voltage has more significant effect on chip temperature, especially when D>50 mm.

Figures 3 (b) and (c) illustrate the changes of chip temperature under varying distances at operating currents of 0.5 A and 0.6 A of the LED module. Chip temperature increases dramatically as operating current increases from 0.4 to 0.6 A under varying driving voltages and distances. In the experiments, an obvious inflection point of chip temperature with respect to distance was observed at D=50 mm under different driving voltages and operating currents. The lowest chip temperatures were observed at 52.4 °C, 58.0 °C, and 68.0 °C under 0.4 A, 0.5 A, and 0.6 A, respectively, at driving voltage of 20 V. At D=50 mm, the microjet achieves optimal heat dissipation in the LED module. When D>50 mm, the increasing rate of chip temperature with respect to distance increased obviously with operating current, especially under low driving voltage. At high operating current of 0.6 A, the incremental increases in chip temperature approximate 44.8 °C, 36.6 °C, 17 °C under 10 V, 15 V, and 20 V, respectively, as D increases from 50 mm to 110 mm.

Figures 4(a) and (b) displays correlations between chip temperature and driving voltage under different operating currents at D=50 mm and D=110 mm, respectively. The experimental results in Fig. 4 (a) show that chip temperature has an approximately linear relationship with driving voltage of the microjet. The decreasing rates of chip temperature with respect to driving voltage are about -1.11, -1.40, and -1.67 using linear fit under 0.4 A, 0.5 A, and 0.6 A, respectively. The measured slopes change slightly with operating currents. Additionally, at D=110 mm, the linear slopes were extrapolated to be -2.84, -3.84, and -4.60, under driving currents of 0.4 A, 0.5 A, and 0.6 A, respectively. The coefficients of determination are from 0.96 to 0.99 for the measured slopes. At D=110 mm, the decreasing rate of chip temperature increases obviously as increasing the operating current.

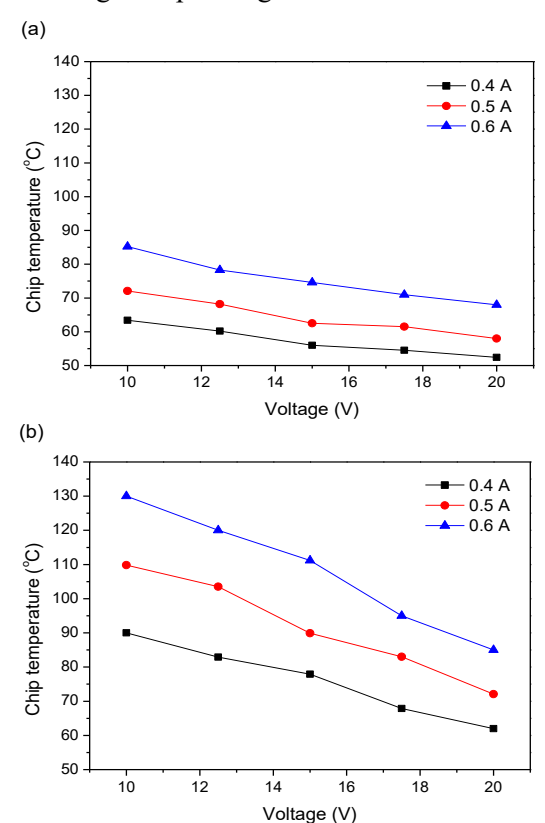


Fig.4. Maximum temperature of the LED modules under different driving voltage at (a) D=50 mm (b) D=110 mm

Figures 5 (a) to (e) reveal thermal images of the LED module under varying driving voltages at D=50 mm and 0.6 A. The LED module is encapsulated by silicone encapsulant to avoid humidity and oxidation from the surrounding. Figure 5(a) shows four high temperature regions on the LED module. To analyze temperature distribution on the LED module, the temperature non-uniformity ΔT is defined as

$$\Delta T = T_{max} - T_{min} \tag{2}$$

in which T_{max} and T_{min} represent the maximum and minimum chip temperature of the LED module. In the experiments, T_{max} and T_{min} are 85.2 °C and 78.1 °C, respectively. The temperature non-uniformity ΔT is about 7.1 °C. Figure 5(b) to 5 (e) show that the ΔT are 6.8 °C, 6.6 °C, 6.3 °C, 5.9 °C under 12.5 V, 15 V, 17.5 V, and 20 V, respectively.

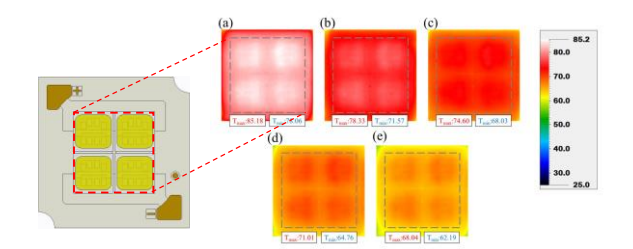


Fig.5. Thermal infrared images on the LED module at varying input voltages (a) 10V (b) 12.5V, (c) 15V, (d) 17.5V, (e) 20V

Figure 6 shows the temperature non-uniformity of the LED module under different driving voltages and operating currents. The temperature non-uniformity decreased with increasing the driving voltages. The higher the operating current results in higher ΔT . The decreasing rate of ΔT with respect to driving voltage shows similar trend under varying currents. The temperature non-uniformity of LED module decreased from 4.9 °C to 4.0 °C and from

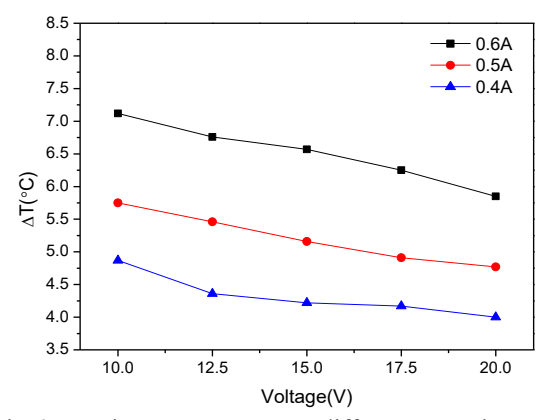


Fig.6. Maximum temperature difference on the LED module at varying input voltages

7.1 °C to 5.9 °C when the driving voltage was increased from 10 V to 20 V under operating currents of $0.4 \, A$ and $0.6 \, A$, respectively.

The input electric power was determined from the current-voltage curve of the LED module. The radiation power of the LED module was measured using an integrating sphere and a spectrometer. During the experiment, LED module was placed on a temperature controller to main constant temperature of 25 °C. The heat power of the LED module is determined by

$$P_{th} = P_e - P_r \tag{3}$$

where P_{th} , P_e , and P_r represented heat power, electric power, and radiation power of the LED module, respectively. Figure 7 shows the heat power, electric power, and radiation power of the LED module under varying driving currents. Heat power of the LED module approximated 0.65 W and 4.75 W under operating current of 0.1 A and 0.6 A, respectively.

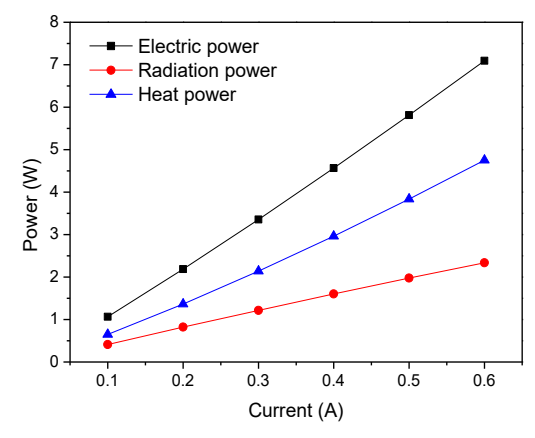


Fig.7. Electric, radiation, and heat power of the LED module under varying driving currents

Figure 8 compares chip temperatures between natural and force convection of the LED module. The heat power of the LED module was increased from 0.65 W to 4.75 W. In this experiment, three different heat dissipation conditions were discussed. Case A is without heat dissipation for the LED module. Case B is to adhesive the LED module on an aluminum heat sink. Case C is to integrate a microjet and a heat sink for the LED module. In Case C, distance and driving voltage were at 50 mm and 20 V, respectively, which provided the optimal cooling performance of the microjet. At low heat power 0.65 W, maximum chip temperatures of the LED module are about 54 °C, 43.5 °C, and 30.9 °C under the conditions of Case A, Case B, and Case C, respectively. Case C can reduce chip temperature by 23.1 °C and 12.6 °C compared with Case A and Case B, respectively. The slopes between chip temperature and heat power approximated 20.6, 11.1, and 8.8 for Case A, Case B, and Case C, respectively, using linear fit (dash lines). To avoid overheating of the LED module, maximum heat power is 2.96 W for Case A. Chip temperature of the LED module approximated 101.4 °C, which approached the maximum rating temperature of the LEDs. For Case C, chip temperature is approximately 49.0

°C and 19.1 °C lower than Case A and Case B, respectively. As heat power increases to 4.75 W, the microjet substantially reduced chip temperature by 21.5 °C compared with only using a heat sink.

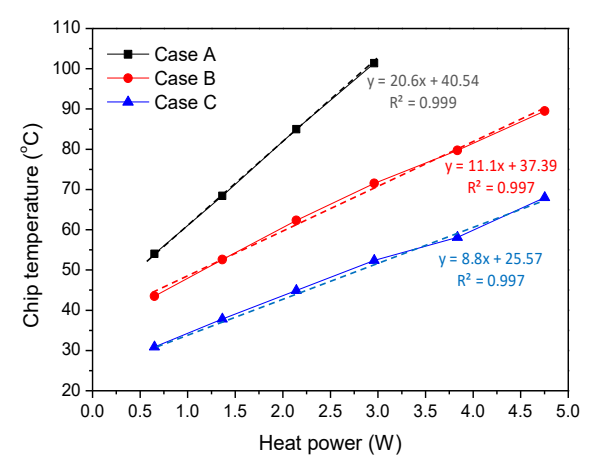


Fig.8. Chip temperatures on the LED module under three different heat dissipation conditions

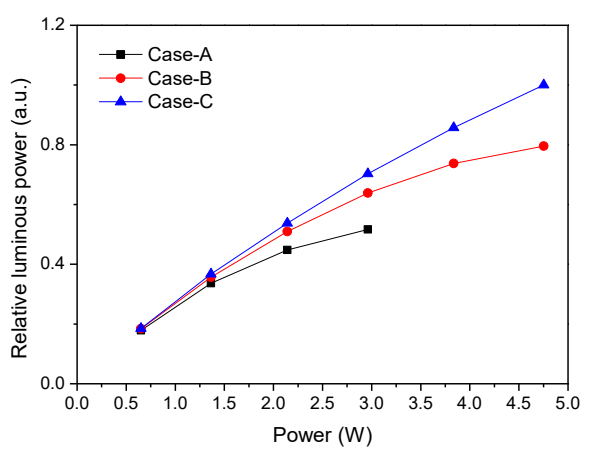


Fig.9. Relative luminous power under varying input power of the LED module for three different heat dissipation conditions

Figure 9 shows the efficiency improvement of using the ultrasonic microjet for the LED module under different heat powers. Compare with Case A and Case B, the use of microjet (Case C) can increase efficiency of the LED module by 18% and 6%, respectively, at heat power of 2.96 W. When the heat power is increased to 4.75 W, Case C revealed a 20% higher efficiency compared to the case with only a heat sink (Case B). The higher the heat power of the LED module, the greater the benefit of using the microjet. According to the experimental results, the ultrasonic microjet

effectively reduces chip temperature, which improves the efficiency of the LED modules.

In order to evaluate heat transfer rate by a piezoelectric micro-blower, Nusselt number and convective heat transfer coefficient are expressed as

$$N_u = \frac{hD}{k} \tag{4}$$

$$h = \frac{P_{th}}{A(T_{LED} - T_{air})} \tag{5}$$

where k is thermal conductivity of air, h is convective heat transfer coefficient. In addition, D is orifice diameter of the microjet, T_{air} is air temperature at 25 °C and A is substrate area. Figure 10 illustrates the Nusselt number as a function of driving voltages. In the experiments, heat power of the LED module was 4.75 W. The figure shows that the Nusselt number increases with driving voltage under varying distance, especially when D= 50 mm. The Nusselt number increased from 7.0 to 9.8 as voltage was increased from 10 to 20 V.

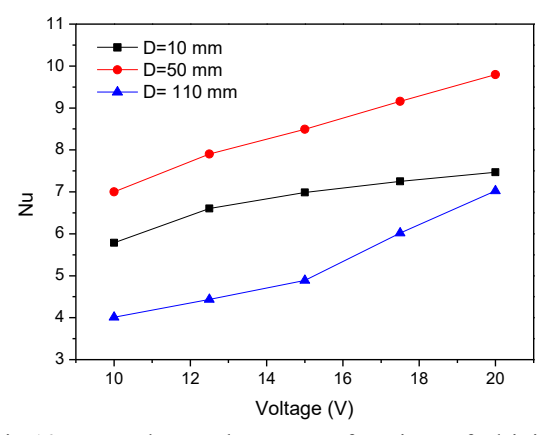


Fig.10. Nusselt number as a function of driving voltage at heat power of 4.75 W

IV. CONCLUSION

This study analyzed the cooling efficiency and performance enhancement achieved when an ultrasonic microjet is used as an active device in a power LED module. Chip temperature is measured using an infrared microscope under varying distances, driving voltages and operating currents. The optimal distance was obtained at D=50 mm under different driving voltages and operating currents. Under the heat

power of 4.75 W, the Nusselt number increased from 7.0 to 9.8 as driving voltage was increased from 10 V to 20 V. When D>50 mm, the increasing rate of chip temperature with respect to distance increased obviously with operating currents, especially under low driving voltage. The slopes between chip temperature and driving voltage had an approximately linear relationship and increased with driving current, especially when D>50 mm. Thermal images reveal that temperature non-uniformity of the LED module decreased with increasing driving voltages and show similar trend under varying operating currents. At high input power of 4.75 W, the microjet effectively reduced chip temperature by 21.5 °C and increased efficiency by 20% compared to an LED module with a heat sink.

REFERENCES

- [1] Qu, J., Wu, H. Y., and Wang, Q., "Experimental Investigation of Silicon-Based Micro-Pulsating Heat Pipe for Cooling Electronics," Nanoscale and Microscale Thermophysical Engineering, Vol. 16, pp. 37-49, 2012.
- [2] Lin, Z., Wang, S., Huo, J., Hu, Y., Chen, J., Zhang, W., and Lee, E., "Heat transfer characteristics and LED heat sink application of aluminum plate oscillating heat pipes," Applied Thermal Engineering, Vol. 31, No. 14-15, pp. 2221-2229, 2011.
- [3] Li, J., Lin, F., Wang, D., and Tian, W., "A loop-heat-pipe heat sink with parallel condensers for high-power integrated LED chips," Applied Thermal Engineering, Vol. 56, No. 1-2, pp. 18-26, 2013.
- [4] Han, Y., Lee, Y. J., and Zhang, X., "Trapezoidal Microchannel Heat Sink with Pressure-Driven and Electro-Osmotic Flows for Microelectronic Cooling," IEEE Transactions on Components, Packaging and Manufacturing Technology, Vol. 3, No. 11, pp. 1851-1858, 2013.
- [5] Silvério, V., Cardoso, S., Gaspar, J., Freitas, P. P., and Moreira, A. L. N., "Design, fabrication and test of an integrated multimicrochannel heat sink for electronics cooling," Sensors and Actuators A: Physical, Vol. 235, No. 1, pp. 14-27, 2015.

- [6] Acikalin, T., Wait, S. M., Garimella, S. V., and Raman, A., "Experimental Investigation of the Thermal Performance of Piezoelectric Fans," Heat Transfer Engineering, Vol. 25, pp. 4-14, 2004.
- [7] Kimber, M., Suzuki, K., Kitsunai, N., Seki, K., and Garimella, S. V., "Pressure and Flow Rate Performance of Piezoelectric Fans," IEEE Transactions on Components, Packaging and Manufacturing Technology, Vol. 32, No. 4, pp. 766-775, 2009.
- [8] Garg, J., Arik, M., Weaver, S., Wetzel, T., and Saddoughi, S., "Meso Scale Pulsating Jets for Electronics Cooling," Journal of Electronic Packaging, Vol. 127, pp. 503-511, 2005.
- [9] Arik, M., "An investigation into feasibility of impingement heat transfer and acoustic abatement of meso scale synthetic jets," Applied Thermal Engineering, Vol. 27, pp. 1483-1494, 2007.
- [10] Park, J., Shin, M., and Lee, C. C., "Measurement of temperature profiles on visible light-emitting diodes by use of a nematic liquid crystal and an infrared laser," Optics Letters, Vol. 29, No. 22, pp. 2656-2658, 2004.
- [11] Wang, C. P., Ying, S. P., Su, Y. C., and Chang, T. L., "Thermal Analysis of Eutectic Flip-Chip Light-Emitting Diodes Fabricated Using Copper-Coated Ceramic Substrate," IEEE Transaction on Electron Devices, Vol. 62, No. 8, pp. 2524-2527, 2015.
- [12] Travnicek, Z., Fedorchenko, A. I., and Wang, A. B., "Enhancement of synthetic jets by means of an integrated valve-less pump: Part I. Design of the actuator," Sensors and Actuators A: Physical, Vol. 120, pp. 232-240, 2005.
- [13] Hsu, S. S., Kordik, J., Travnicek, Z., and Wang, A. B., "The Performance of Hexzgonally Arranged Hybrid Synthetic Jets," Journal of Flow Visualization and Image Processing, Vol. 19, pp. 1-13, 2012.
- [14] Dau, V. T., and Dinh, T. X., "Numerical study and experimental validation of a valveless piezoelectric air blower for fluidic applications," Sensors and Actuators B: Chemical, Vol. 221, pp. 1077-1083, 2015.
- [15] Chung, H. C., Kummari, K. L., Croucher, S. J., Lawson, N. J., Guo, S., Whatmore, R. W., and Huang, Z., "Development of

- piezoelectric fans for flapping wing application," Sensors and Actuators A: Physical, Vol. 149, No. 1, pp. 136-142, 2009.
- [16] Lin, C. N., "Analysis of three-dimensional heat and fluid flow induced by piezoelectric fan," International Journal of Heat and Mass Transfer, Vol. 55, pp. 3043-3053, 2012.
- [17] Li, H. Y., Chao, S. M., Chen, J. W., and Yang, J. T., "Thermal performance of plate-fin heat sinks with piezoelectric cooling fan," International Journal of Heat and Mass Transfer, Vol. 57, No. 2, pp. 722-732, 2013.
- [18] Ma, H. K., Su, H. C., and Luo, W. F., "Investigation of a piezoelectric fan cooling system with multiple magnetic fans," Sensors and Actuators A: Physical, Vol. 189, No. 15, pp. 356-363, 2013.
- [19] Fukue, T., Hirose, K., and Terao, H., "Cooling Performance of Impinging Jet from Piezoelectric Micro Blower mounted in Narrow Flow Passage," International Conference on Electronics Packaging and iMAPS All Asia Conference, pp. 605-610, 2015.
- [20] Ghaffari, O., Solovitz, S. A., Ikhlaq, M., and Arik, M., "An investigation into flow and heat transfer of an ultrasonic microjet device for electronics cooling applications," Applied Thermal Engineering, Vol. 106, No. 5, pp. 881-889, 2016.
- [21] Chovet, C., Lippert, M., Keirsbulck, L., and Foucaut, J.-M., "Dynamic characterization of piezoelectric microjets for separation flow control," Sensors and Actuators A: Physical, Vol. 249, No. 1, pp. 122-130, 2016.
- [22] Wang, C. P., Wang, G. B., and Ting, Y., "Analysis of dynamic characteristics and cooling performance of ultrasonic microjet," Microelectronic Engineering, Vol. 195, pp. 1-6, 2018.
- [23] Yung, K. C., Liem, H., and Choy, H. S., "Heat transfer analysis of a high-brightness LED array on PCB under different placement configurations," International Communications in Heat and Mass Transfer, Vol. 53, pp. 79-86, 2014.
- [24] Canale, L., Dupuis, P., Leng, S., and Zissis, G., "Study of High-Brightness LED

Samples Aged Under Stress Temperature Conditions: Electrical Characterizations and Signature Evolution Analysis," IEEE Transactions on Industry Applications, Vol. 52, pp. 502-510, 2016.